論文内容の要旨

論文題目　Microscopic observations of calcite dissolution and crystal growth:
An insight into the interaction between aspartic acid and calcite surface

（カルサイトの溶解及び結晶成長の観察から解き明かす
アスパラギン酸分子とカルサイト結晶表面との相互作用）

氏名　吉野　徹

Calcium carbonate is a major biomineral which can be found as crystalline or amorphous materials produced by living organisms. The biomineral of calcium carbonate has been focused in various scientific fields. Previous studies suggested that acidic biomolecules (peptides, polysaccharides, and phosphate compounds) serve an important role in the process of biomineralization. Regarding peptides, aspartic acid (Asp)-rich peptides might control polymorphism and structure of calcium carbonate, which implies that interactions between carboxylate and the calcium carbonate surface are important to elucidate biomineralization mechanisms. In this study, the interaction was evaluated from the observation of the calcite ($CaCO_3$) dissolution and crystal growth processes in the Asp additive solution using microscopic methods.

In chapter 2, the calcite dissolution in the Asp additive or absent solution under the surface controlled kinetics was observed using an atomic force microscope (AFM) and a confocal laser scanning microscope (CLSM) to clarify the interaction between Asp and the calcite surface. The step velocities of each step constructing etch-pit were determined from the in-situ observation using AFM. I developed an AFM flow through system to realize the surface controlled kinetics. Using a meniscus type AFM fluid cell and optimizing flow rate realized the surface controlled kinetics and enabled me to evaluate the interaction which is a surface process (Fig.1). The dissolved calcite specimens were observed using CLSM in air to obtain the precise etch-pit morphology. The morphology data were used to eliminate systematic errors in the measured step velocities, which derive from an instrumental drift of piezoscanner during the scanning. All influent solutions were adjusted to pH = 8.00 and I = 0.1 M. All runs were performed at room temperature (25±1°C).

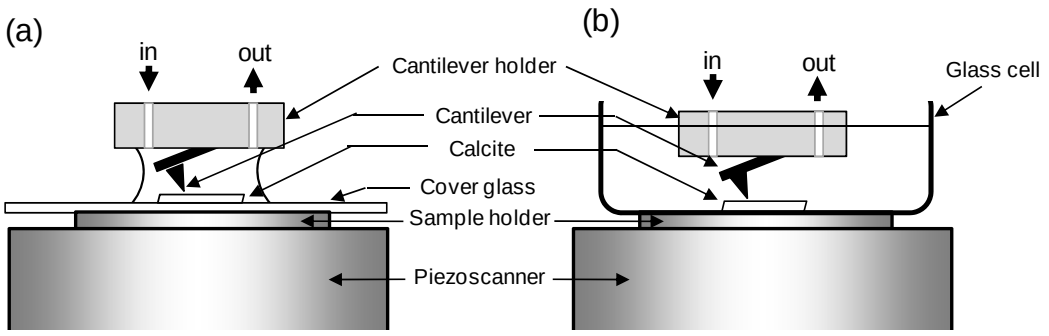

Fig.1 A schematic illustration of AFM fluid cells
(a) The meniscus type fluid cell for the surface controlled kinetics (b) The cylinder type AFM fluid glass cell for the mixed kinetics

The etch-pit shape changed drastically depending on the L-Asp concentration ([L-Asp]) (Fig.2). Fig.2g presents a schematic illustration of an ideal calcite etch-pit and an observed etch-pit at [L-Asp] = 0.1 M, where obtuse steps (+) and acute steps (−), respectively, are defined as those having intersections with (104) at angles of 102° and 78°. The etch-pit shape changed from rhombus to pentagon and to triangle (not perfectly, retaining an extra step) with increased [L-Asp]. A previous report has already described that the triangular etch-pit shape emerged in the 0.1 M L-Asp aqueous solution, but the formation of pentagonal etch-pits at [L-Asp] of 0.03–0.07 M was found for the first time in this study. The pentagonal etch-pits resulted from changes of obtuse step directions and appearance of [010] steps. The obtuse step directions were changed continuously from $[\underline{4}41]_+$ ($[48\underline{1}]_+$), to $[\underline{4}21]_+$ ($[46\underline{1}]_+$) with increased [L-Asp]. These results indicated that affinities of L-Asp to the obtuse and the [010] steps are stronger than those to the acute steps.

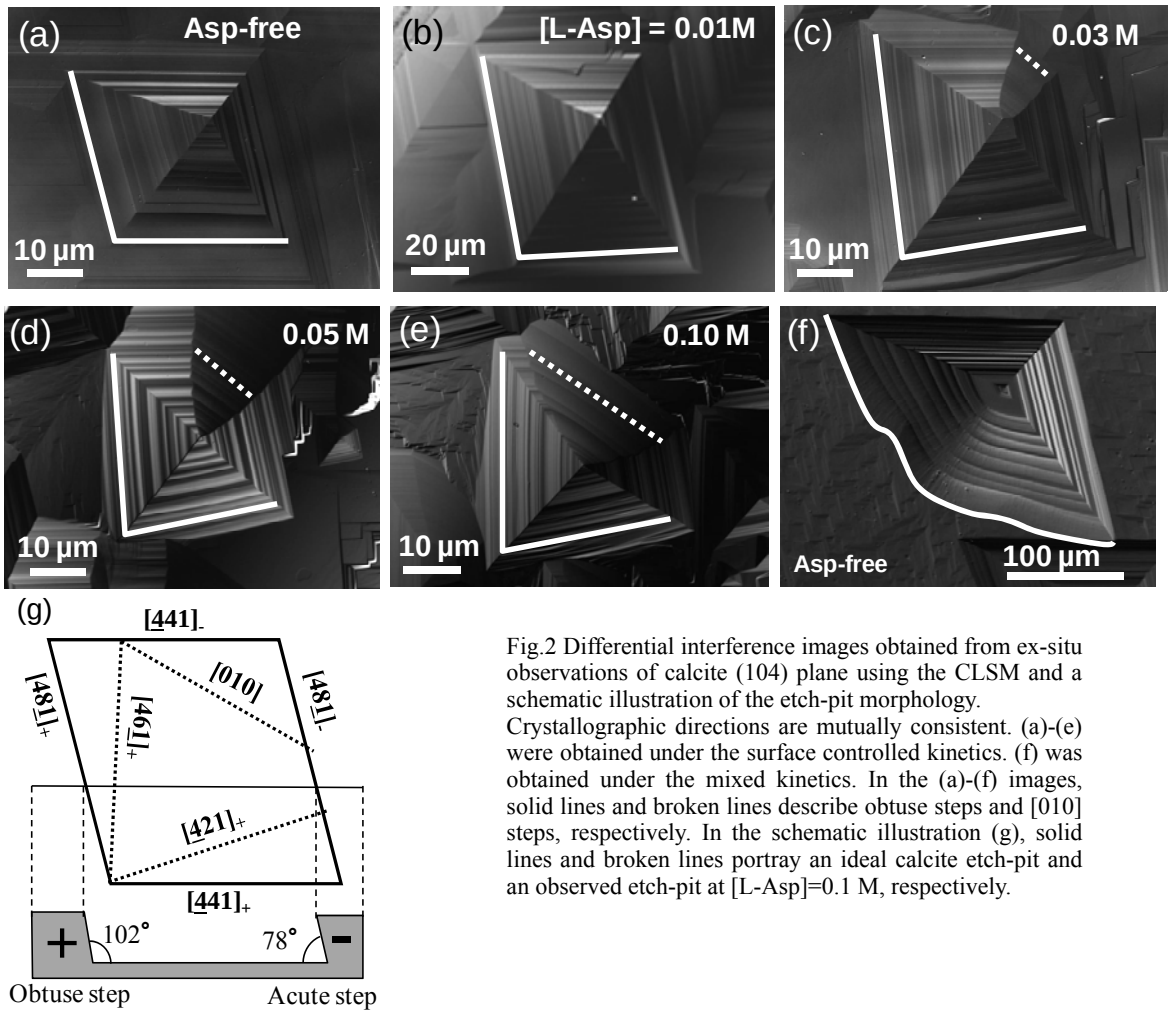

Fig.2 Differential interference images obtained from ex-situ observations of calcite (104) plane using the CLSM and a schematic illustration of the etch-pit morphology.
Crystallographic directions are mutually consistent. (a)-(e) were obtained under the surface controlled kinetics. (f) was obtained under the mixed kinetics. In the (a)-(f) images, solid lines and broken lines describe obtuse steps and [010] steps, respectively. In the schematic illustration (g), solid lines and broken lines portray an ideal calcite etch-pit and an observed etch-pit at [L-Asp]=0.1 M, respectively.

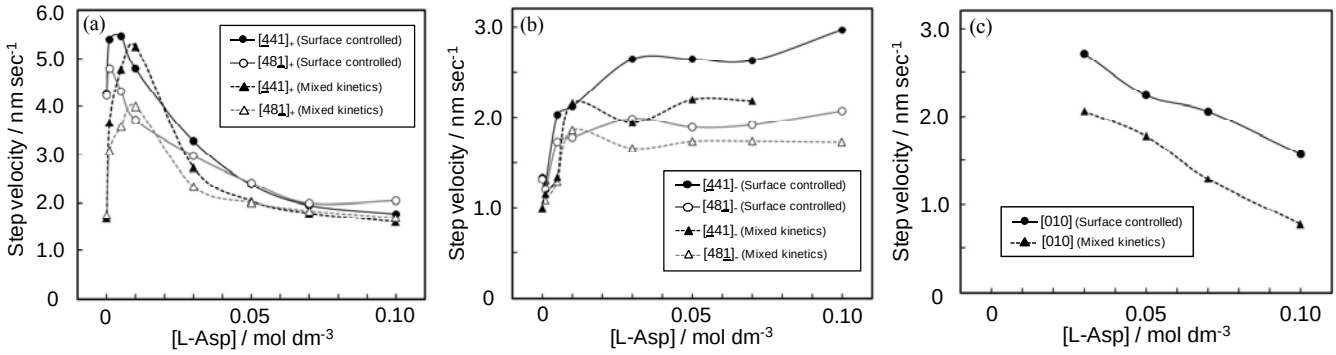

Fig.3 L-Asp concentration dependence of the step retreat velocities of obtuse steps (a), acute steps (b), and [010] step (c).

Fig.3 shows L-Asp concentration dependence of the step retreat velocities. At lower L-Asp concentrations, all the step retreat velocities increased concomitantly with increased [L-Asp]. I concluded that the increase was attributable to the promotion of the surface process triggered by L-Asp, which has been reported in the crystal growth studies. The present study first clarified that L-Asp promotes the surface process also in the dissolution of calcite. At higher L-Asp concentrations, the step retreat velocities were classifiable into two cases: (1) decreasing concomitantly with increased [L-Asp] (obtuse and [010] steps), (2) constant irrespective of [L-Asp] (acute steps).

The decrease of obtuse and [010] step retreat velocities by the addition of L-Asp could be explained from a kink blocking effect of L-Asp. The reactive kink sites were blocked by the adsorption of L-Asp and it led to the decrease of step retreat velocities. The preferential adsorption of L-Asp to the steps was consistent with the results of morphological change of etch-pit.

The step retreat velocities were different between symmetrical steps ($[\underline{4}41]_{\pm}$ and $[48\underline{1}]_{\pm}$ steps). Fig.3 shows that the step retreat velocities of $[\underline{4}41]_{\pm}$ steps are faster than those of $[48\underline{1}]_{\pm}$ steps at almost all [L-Asp] conditions. This asymmetry has been reported by Orme *et al*. (2001). They indicated the difference of binding energy between enantiomers of Asp (L form and D form) to the $[\underline{4}41]_{\pm}$ (or $[48\underline{1}]_{\pm}$) step edges on the calcite cleavage surface from the calculation. Moreover, they demonstrated that the growth hillock shapes formed in the presence of L- and D-Asp were mirror images of one another. In the present study, the relation could be observed between the etch-pit shapes formed in L-Asp and D-Asp aqueous solution (Fig.4). Based on the inhibitive effects of Asp, the lower step velocities mean the stronger affinity of Asp to the step. Therefore, I concluded that L-Asp prefers the $[48\underline{1}]_{\pm}$ steps to the $[\underline{4}41]_{\pm}$ steps. This result was consistent with the result of Orme *et al*. (2001). It was also confirmed that the preferences were inversed in the case of D-Asp.

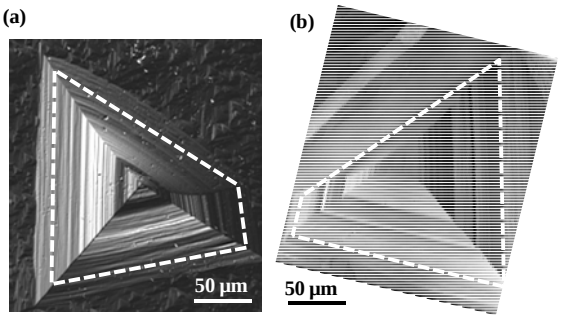

Fig.4 CLSM images of etch-pits formed in 0.1 M Asp solutions. (a) L-Asp (b) D-Asp.

In chapter 3, the calcite dissolution under the mixed kinetics, which means that the dissolution rate is controlled by surface and transport processes, was observed using AFM and CLSM. The mixed kinetics was realized by improvement of the AFM fluid cell. In the experiment, the AFM fluid cell was substituted to the cylinder glass cell for the meniscus cell (Fig.1). The internal volume of the cylinder glass cell was much greater than that of the meniscus cell. The larger volume led to the longer residence time of the solution, and

resulted in the mixed kinetics. The observations were carried out under the same conditions that used in the chapter 2 except for the rate determining step.

At the lower L-Asp concentration, the increase of step retreat velocities was much greater than that under the surface controlled kinetics, and could not be explained from the promotion of surface process alone (Fig.3). It indicated that the promotion effects appeared not only in the surface process but also in the transport process. The rounded etch-pit has been observed at Asp-free condition under the mixed kinetics (Fig.2f). However, the rounding disappeared with the decrease of residence time or the addition of L-Asp. The similarity between the effects of residence time and L-Asp on the rounding supported the promotion effect of L-Asp on the transport process.

In chapter 4, the crystal growth of calcite was observed using AFM. The supersaturation dependence of step velocities was determined from the in situ AFM observation to clarify the mechanism of the inhibitive effect of L-Asp on the step progress. In this experiment, the calculation of the supersaturation in the Asp-$CaCO_3$ system was improved to obtain the precise value. Moreover, Time-of-Flight Secondary Ion Mass Spectrometry (ToF-SIMS) analysis was carried out to directly detect adsorbed L-Asp on the calcite surface.

The addition of L-Asp modified the growth hillock morphology on the calcite surface. The rounding appeared in acute and obtuse steps. At [L-Asp] = 1 mM, driving force dependence of acute step velocities indicated that the inhibitive effect of L-Asp was kink-blocking. Based on the Terrace-Ledge-Kink model, the rounding steps derived from kink accumulations. ToF-SIMS analysis could not detect L-Asp on the calcite surface and in the calcite crystal. In the ToF-SIMS analyses, the estimated detection limit of L-Asp was 0.01 mol%. This result supported the kink blocking as the inhibitive effects because the kink site is the fewer site compared to terrace and step edge.

The observations of the calcite ($CaCO_3$) dissolution processes in the L-Asp additive solution using AFM and CLSM clarified the preferential adsorption of L-Asp to each step. Firstly, the affinities of L-Asp to the obtuse and the [010] steps were greater than to the acute steps. Secondly, those of L-Asp (D-Asp) to the $[48\underline{1}]_{\pm}$ ($[\underline{4}41]_{\pm}$) were greater than to the $[\underline{4}41]_{\pm}$ (**(**$[48\underline{1}]_{\pm}$). The results of step retreat velocities measured under the two kinetic conditions indicated the promotion effect of L-Asp to the surface process and transport process, and the inhibitive effect of L-Asp by blocking to the reactive kink sites. The kink-blocking effect was supported by the crystal growth study and the ToF-SIMS analysis. This study demonstrates that the complementary approach from the dissolution and crystal growth studies can be a promising approach to elucidate the interaction.